The interplay between grain boundary structure and defect sink/annealing behavior

To cite this article: J Han *et al* 2015 *IOP Conf. Ser.: Mater. Sci. Eng.* **89** 012004

The interplay between grain boundary structure and defect sink/annealing behavior

J Han[1], V Vitek[1], and D J Srolovitz[1,2]

[1]Department of Materials Science and Engineering, University of Pennsylvania, 3231 Walnut St., Philadelphia, PA 19104 USA
[2]Department of Mechanical Engineering and Applied Mechanics, University of Pennsylvania, 3231 Walnut St., Philadelphia, PA 19104 USA

E-mail: srol@seas.upenn.edu

Abstract. We present a series of results from atomistic simulations in three different materials (3 crystal structures) that demonstrate that the multiplicity of grain boundary (GB) structures at fixed macroscopic GB degrees of freedom is both extremely large and ubiquitous. The GB energy vs. misorientation curve that is commonly discussed is in fact a wide band, with many GB states very close in energy. The existence of so many GB states suggests that GB configurational entropy S_c is important for GB properties. We demonstrate that the GB S_c consists of two major contributions, one of which is geometric in nature and one that depends on bonding. We then show how this concept can be employed to predict GB relaxation dynamics by analogy with Adam-Gibbs theory, originally derived to predict the properties of glass forming liquids. Finally, we apply these predictions to understand GB denuded zone size during irradiation.

1. Introduction

Grain boundaries are widely thought of as being perfect sinks and/or sources of defects in polycrystals. Two classical examples are grain boundaries as sinks for vacancies or interstitials during irradiation damage or in creep and grain boundaries behaving as sinks for dislocations. As the dislocation example illustrates, absorbing dislocations changes grain boundary structure because net Burgers vector can neither be created nor destroyed. When a dislocation enters a grain boundary it can lower its energy by decomposing into partial (grain boundary) dislocations with Burgers vectors much smaller than are possible in the crystal, consistent with the DSC (displacement shift complete) lattice [1]. Such DSC dislocations change the boundary structure.

There are many examples in the literature (e.g., see [2-6]) of the existence of multiple grain boundary structures corresponding to the same five macroscopic bicrystal parameters. Some more recent examples include dislocation pairing in low angle grain boundaries [7] and the observation of grain boundary structural phase transitions [8]. Structural multiplicity is a general feature of grain boundaries [9]. The existence of multiple grain boundary structures is not determined by the structure of the coincidence site lattice alone, since not all symmetry-allowed structures are stable.

In this paper, we discuss the multiple possible structures of a grain boundary of fixed macroscopic degrees of freedom, elucidate the implications of these for grain boundary thermodynamics and kinetics, including the case of adsorption of point defects as occurs, for example, during radiation damage. We do this via application of atomistic simulation techniques and to demonstrate the generality of the results we consider a set of symmetric tilt grain boundaries over the full angular range for materials with three

different crystal structures and two types of atomic bonding. Finally, we compare experimental and predicted point defect adsorption kinetics in a radiation damage environment.

2. Multiplicity of Grain Boundary Structures

Metastable GB structures correspond to local minima in the potential-energy landscape for fixed macroscopic bicrystal geometry. To describe an elemental (or disordered solid solution) bicrystal, five macroscopic geometrical degrees of freedom (DOFs) are required; they can be represented by a rotation axis $\boldsymbol{o}$ (2), a rotation angle θ (1), and the GB plane normal $\boldsymbol{n}$ (2). Any atomistic description of a GB in a bicrystal must also account for three microscopic geometrical DOFs: the rigid-body displacement of two adjoining crystals with respect to each other [1]. Such displacement has two components, t_1 and t_2, parallel to the GB plane and one component, t_3, perpendicular to the plane. The latter represents expansion or contraction of the bicrystal. For a given t_1 and t_2, t_3 is determined uniquely by energy minimization, leaving only $\boldsymbol{t} \equiv (t_1, t_2)$ as the free microscopic DOFs. In a grand-canonical ensemble another microscopic DOF arises. This involves adding/removing atoms to/from the GB, i.e., changing the GB atomic fraction, φ [10]. Adding/removing a monolayer of atoms to/from the GB plane simply shifts one grain relative to the other. Hence, the GB structure repeats as the GB atomic fraction, $\varphi \equiv$ (number of added atoms)/(number of atoms per monolayer), varies from 0 to 1. Changes in φ may lead to additional metastable structures [8,10]. Therefore, metastable GB structures can be found by minimizing the energy of a bicrystal model with respect to the atomic coordinates and the variables $\boldsymbol{t}$ and φ for fixed macroscopic DOFs. Energy minimization starting from different initial translation states $\boldsymbol{t}$ with certain atomic fraction φ may result in different metastable states, characterized by $(\boldsymbol{t}^{(i)},\varphi^{(i)})$, where the superscript (i) represents one of the N accessible metastable GB states for fixed $\{\boldsymbol{o},\theta,\boldsymbol{n}\}$.

For given macroscopic DOFs, different metastable GB structures may be found for different $\boldsymbol{t}$ and

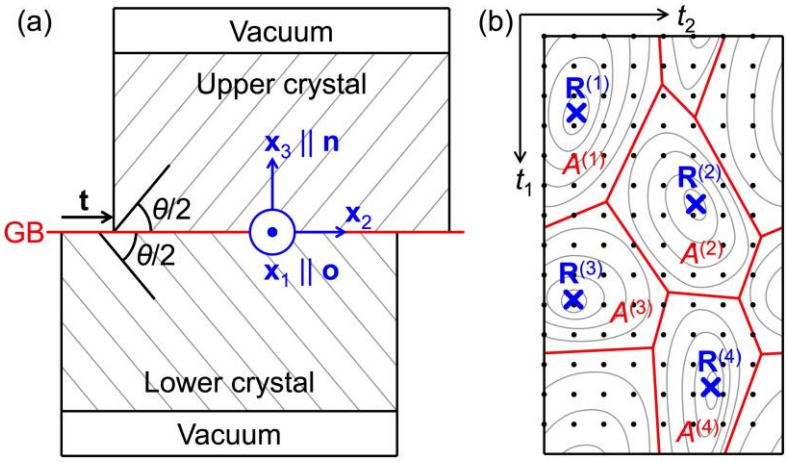

Figure 1. (a) Schematic of the simulation supercell; here, we use $\boldsymbol{o}$ = [001] and focus on symmetric tilt boundaries. (b) Schematic of the sampling of translation GB states (points) and the associated GB energy contours (gray curves) in the periodic GB cell. $\boldsymbol{R}^{(i)}$ denotes the i^{th} metastable structure found for a metabasin of area $A^{(i)}$ that is delimited by dividing surfaces marked by red lines.

φ; this is called GB structural multiplicity. It has been observed in both experiments and atomistic simulations [8-14]. There is evidence that GB structural multiplicity holds the key to understanding such dynamic phenomena as GB sliding [3] and point-defect absorption at GBs [8, 11]. However, at present the idea of structural multiplicity has only been used to explain microscopic mechanisms rather than predict properties. Here we propose a novel approach to predict nonequilibrium GB structures and properties, accounting for the important effect of GB structural multiplicity.

As illustrated in Fig. 1(a), a series of symmetric tilt GBs in cubic materials were constructed by

rotating two crystals with respect to each other by ±θ/2 about the axis $\boldsymbol{o}$ = [001] and joining them at the plane with normal $\boldsymbol{n}$ = [010]; the indices refer to the unrotated crystals. Using this approach, we constructed 110 coincidence-site-lattice GBs with $0° \leq \theta \leq 90°$ and reciprocal coincident site density of $\Sigma \leq 941$. The simulation supercells were created as shown in Fig. 1(a). Periodic boundary conditions were applied along x_1 and x_2 and there was a vacuum above and below the bicrystal (in x_3). The thickness of each crystal along x_3 was 60-80 nm. To determine the generality of the results, we considered three model materials with different crystal structures and bonding: embedded atom-method (EAM) Al [15] (fcc), Finnis-Sinclair (FS) W [16] (bcc), and Tersoff Si [17] (diamond cubic).

To investigate the effect of microscopic DOFs, the initial GB configurations were explored by uniformly sampling the translation $\{\boldsymbol{t}\}$ space for each misorientation θ (see Fig. 1(b)). To do this, one crystal was rigidly displaced by the vector $\boldsymbol{t}$ with respect to the other until the vector swept the entire periodic GB cell. The density of the sampled configurations in the periodic GB cell area A_{cell} is $94a_o^{-2}$ for Al and W, and 257 a_o^{-2} for Si (a_o is the cubic lattice constant). For each configuration, the energy

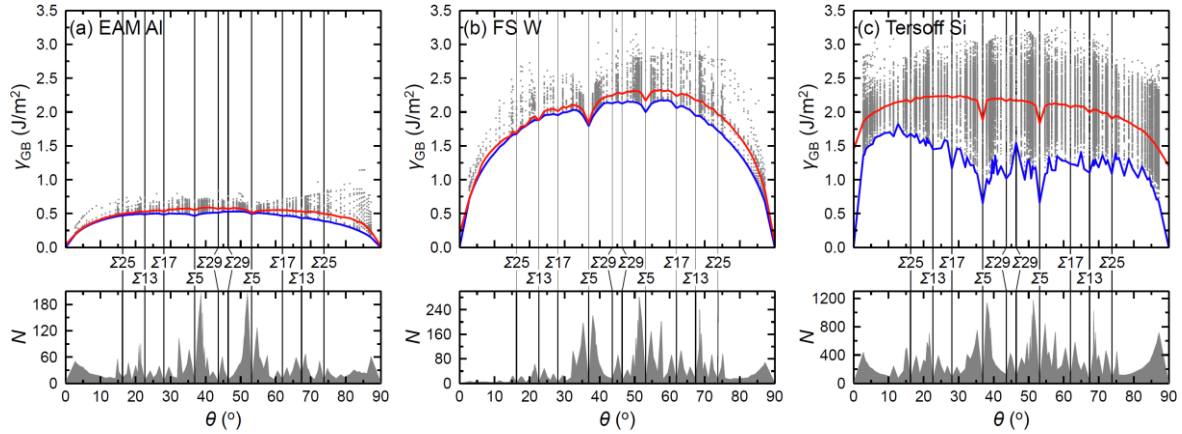

Figure 2. GB energy γ versus misorientation θ for a series of [001] symmetrical tilt GBs in (a) EAM Al (fcc), (b) FS W (bcc), and (c) Tersoff Si (diamond cubic). In the top panel each data point represents the GB energy associated with one metastable structure $\gamma^{(i)}$ (corresponding to the translation $t^{(i)}$); the blue curves denote the lowest energies $\gamma_{\text{min}}(\theta)$ and the red curves denote the basin-ensemble-averaged GB energies $\langle \gamma(\theta) \rangle$, as defined in Section (3). The lower panel shows the number of metastable GB states $N(\theta)$. The vertical lines label the misorientations with $\Sigma < 30$.

was minimized with respect to the atomic coordinates and translation vector $\boldsymbol{t}$ using a steepest descent procedure. GB configurations with different initial $\boldsymbol{t}$ relaxed into a finite set of translation states corresponding to local minima in the GB energy with respect to $\{\boldsymbol{t}\}$ (stable or metastable structures). Associated with each translation $\boldsymbol{t}^{(i)}$ is a particular metastable GB with energy $\gamma^{(i)}$ and a basin of attraction (metabasin) within which any sampled configuration relaxes into the same structure $\boldsymbol{R}^{(i)}$.

The energy of each metastable structure $\gamma^{(i)}$ is shown in the top panel of Fig. 2 as a function of misorientation θ. The minimum-energy structures possess the energy γ_{min} (blue curves in the top panel of Fig. 2). The $\gamma_{\text{min}}(\theta)$-curves for Al and W feature a series of cusps at misorientations corresponding to small Σ values [18] while the curve for Si is highly serrated with particularly sharp cusps at two Σ5 GBs. For nearly all misorientations, multiple metastable states exist, each with a unique energy. Then, considering all accessible states, we see that the classical GB energy versus misorientation curve broadens into a GB-energy band (γ-band). The existence of such finite energy bands has been neglected in most earlier studies of GB properties.

The thickness/width of a γ-band varies considerably from material to material, as seen in Fig. 2. The band width for a GB with misorientation θ is $\Delta(\theta) \equiv \gamma_{max}(\theta)-\gamma_{min}(\theta)$, where $\gamma_{max/min}(\theta)$ is the maximum/minimum energy amongst all metastable GBs with θ. The average band width $\langle\Delta\rangle$ and the average relative width $\langle\delta\rangle \equiv \langle\Delta\rangle/\gamma_{min}$ over all θ values were found to be $\langle\Delta\rangle$ = 0.27, 0.66 and 1.6 J/m^2, and $\langle\delta\rangle$ = 0.80, 0.40 and 1.4 for Al, W and Si, respectively. The GB-energy variation in Si is the largest. Al exhibits smaller $\langle\Delta\rangle$ value but larger $\langle\delta\rangle$ value than W. These differences may stem from differences in bonding amongst these materials; covalent bonds in Si may stabilize more metastable GB structures than metallic bonds. Another measure of a γ-band is the number of metastable GB states $N(\theta)$ (the bottom panels of Fig. 2). Examination of the $N(\theta)$ curves shows a strong similarity amongst the three model materials. Such material-independence is related to the geometric nature of GB configurational entropy (see below).

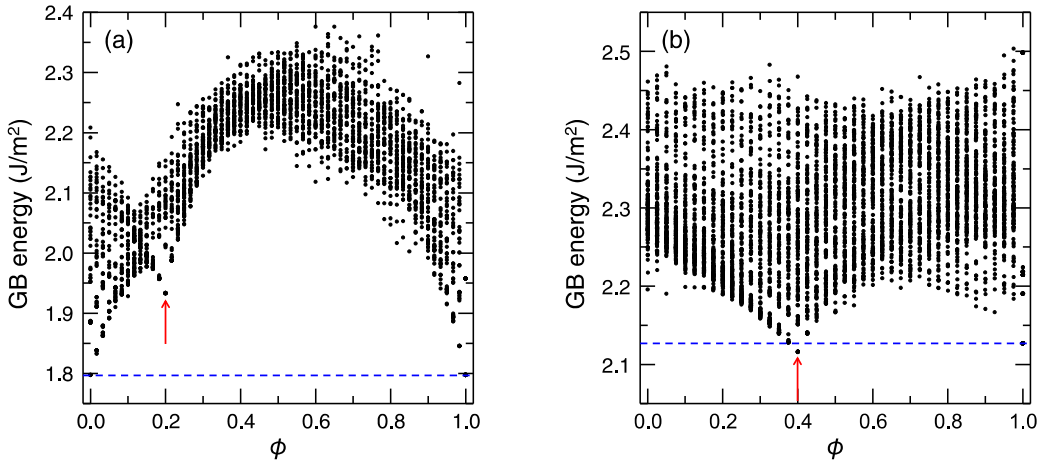

Figure 3. GB energies as a function of atomic fraction φ for (a) Σ5 36.9˚ (310) and (b) Σ29 46.4˚ (730) GBs in W. Each data point corresponds to a different metastable translation state t. The new metastable states identified by varying φ are indicated by the red arrows. The horizontal dashed blue lines indicate the lowest energies found by translations alone (φ = 0).

Atoms can be added to or removed from a grain boundary (GB) without changing its macroscopic bicrystallography (misorientation, boundary inclination) or translational state. The GB atomic fraction φ is varied by adding or removing atoms in the GB plane; adding a full atomic plane (parallel to the GB) does not change the GB structure. We investigated this additional degree of freedom (DOF) following the non-conservative sampling method proposed by Frolov *et al.* [8]. We examined Σ5 36.9˚ (310) and Σ29 46.4˚ (730) GBs in W in the full $\{\boldsymbol{t}, \varphi\}$ space, where 60 and 40 fundamental GB cells were in the GB simulation cell, respectively. The GB-energy spectrum as a function of φ and $\boldsymbol{t}$ is shown in Fig. 3 for these GBs. Introducing φ as a variable produces, in each case, exactly one additional metastable state (i.e., one for which γ is a minimum with respect to $\boldsymbol{t}$ and φ). The extra minimum for the Σ5 (310) GB corresponds to a metastable GB state, whereas in the Σ29 (730) case the new structure has even lower energy than the structures created by translations alone (i.e., φ = 0). Note, the points in these plots not corresponding to the bottom of the cusps do not represent new GB structures, but rather one of the metastable GBs with a non-periodic array of point defects. Since adding additional atoms to the GB rarely add more than a single additional metastable state, we neglect those found from varying φ in the GB statistics, below.

The metastable states in the grain boundary bands in Fig. 2 are not arbitrary, but are closely related to the GB structure. The structure of grain boundaries can be well described within the structural unit

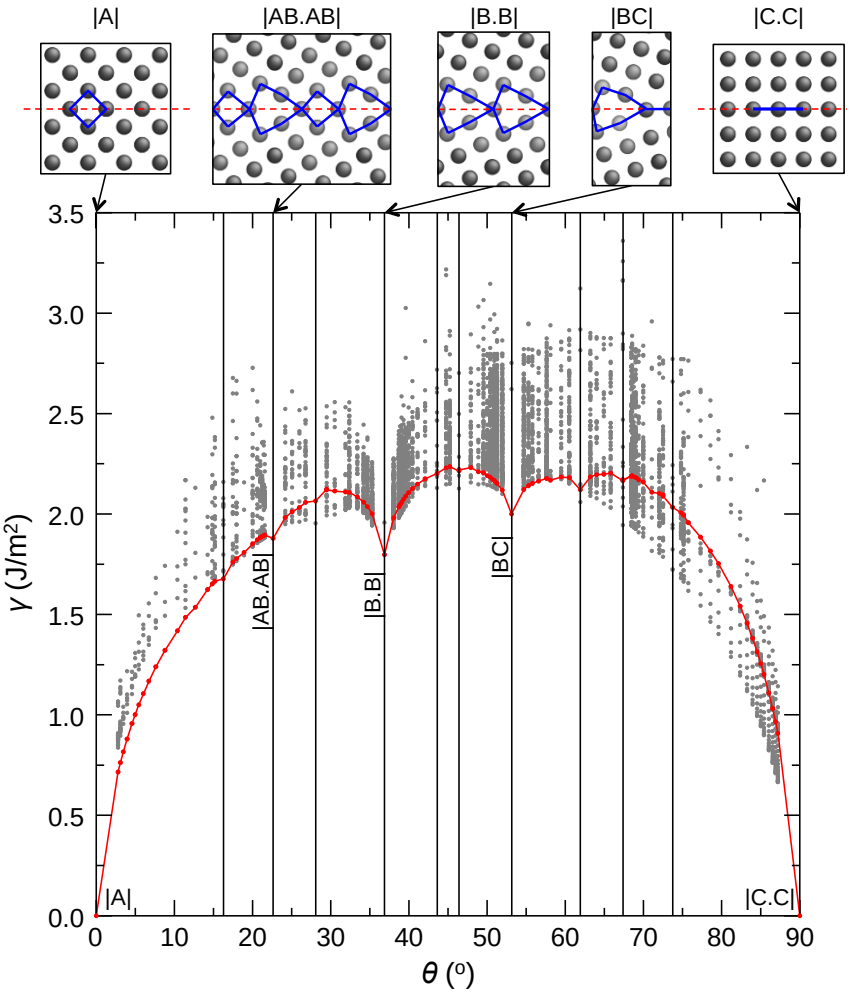

Figure 4. The grain boundary energy band structure from Fig. 2b for W. The red curve shows a path through the individual stable (or metastable) states that correspond to combinations of the structural units A for 0˚ and the Σ5 boundary (37˚) structural units B and between 37˚ and 90˚ a combination of C units.

(SU) model (e.g., see [19, 20]), which posits that GBs are composed of a periodic array of a single fundamental structural unit in the case of certain high symmetry boundaries at specific misorientations (corresponding to cusps in a GB energy versus misorientations plot) and for misorientations between these delimiting boundaries the structure is composed of an arrangement of the two types of structural units found in the delimiting boundaries composed of single SUs. Consider the energy band structure of the relatively simple case of the symmetric [001] tilt GBs in W, which is shown in Fig. 2b. Boundaries corresponding to the red curve between 0˚ and 37˚ (a Σ5 boundary) consist entirely of the structural units from these two end points as shown in Fig. 4. The 0˚ and 37˚ boundaries correspond to A and B SUs, respectively, and for all of the misorientations in between, the boundary structures delineated by the red curve indicate, boundaries that are solely composed of A and B SUs. For misorientations between 37˚ and 90˚ the GBs are solely composed of B and C units. Since units A and B correspond to perfect crystals, there is only one "boundary" type at 0˚ and 90˚. For the 37˚ Σ5 GB, there are three possible GB structures (1 of these is associated with changing φ) and so, in principle, there should be three distinct paths through the metastable states corresponding to combinations of A and B, and A and B' for the misorientations range between 0˚ and 37˚. However, there are clearly more than two possible paths; i.e., there are many metastable GB structures at misorientations between these two limits. This implies

that there are other delimiting boundaries, consisting of repeating (complex) unit cells at misorientations between 0˚ and 37˚ degrees that are represented by very small cusps in the GB energy versus misorientations plot. All of the metastable states seen in Figs. 2 and 4 can be connected through such a SU model construction.

3. Grain Boundary Statistics

The results presented above demonstrate that for grain boundaries with almost any set of macroscopic degrees of freedom, there are many possible, metastable grain boundary structures and a correspondingly many possible grain boundary energies. This raises the question, which grain boundary structure or which distribution of structures will be observed in experiments. The answer will obviously be different depending on whether or not the grain boundary is in equilibrium. If the grain boundary is not in equilibrium, the structure or distribution of structures will be sensitive to such things as how the polycrystals were synthesized, the thermal history of the polycrystals, and grain boundary dynamical processes operative at the time the structure is observed (or immediately prior to quenching) such as grain boundary migration, grain boundary sliding, etc.

In equilibrium (annealing over infinite time), the distribution of grain boundary structures should be determined by the Boltzmann statistics. The probability of observing a grain boundary in the state i, $p_e^{(i)}(\theta) = \exp(-E^{(i)}(\theta)/kT) / Z$, where $E^{(i)}(\theta) = A_{cell}\,\gamma^{(i)}(\theta)$, kT is the thermal energy, and Z is the partition function. The blue curves in Fig. 2 correspond to the equilibrium internal energies of the grain boundaries as a function of misorientation at zero Kelvin (in this case, the only GB structures observed correspond to the minimum energy structures). At finite temperature, the average grain boundary energy is $\langle\gamma(\theta)\rangle_{\mathrm{e}} = \Sigma_i\, p_e^{(i)}(\theta)\gamma^{(i)}(\theta)$, where the summation is over all $N(\theta)$ GB states and $p_e^{(i)}$ is evaluated at the temperature of interest. We can also consider an extreme non-equilibrium (xne) state, where the probability of a particular GB state is determined by the size of the GB translations phase space it occupies, that is $p_{xne}^{(i)} = A^{(i)}/A_{cell}$, where $A^{(i)}$ is the area of the basin of attraction corresponding to state i and A_{cell} is the area of the entire translation space as seen in Fig. 1b. The red curves in Fig. 2 corresponds to the average grain boundary energy for this ensemble; i.e., $\langle\gamma(\theta)\rangle_{\mathrm{xne}} = \Sigma_i\, p_{xne}^{(i)}(\theta)\gamma^{(i)}(\theta)$. Examination of the results in Fig. 2c for Si, shows that while the equilibrium grain boundary energy (blue curve) shows a rapid oscillation with θ not normally observed in experiments, the non-equilibrium grain boundary energy (red curve) shows a relatively smooth variation with θ except for the cusps observed at low Σ (i.e., Σ5), as commonly seen in experiments. This difference between equilibrium and extreme non-equilibrium is not as strong for Al or W. In most non-equilibrium situations, we expect that the average grain boundary energy is $\langle\gamma(\theta)\rangle_{\mathrm{e}} < \langle\gamma(\theta)\rangle < \langle\gamma(\theta)\rangle_{\mathrm{xne}}$ (this is, however, not a rigorous statement).

The presence of a large number of possible grain boundary structures can be described through the configurational entropy, as defined in information theory (i.e., the Shannon entropy [21]). For the extreme non-equilibrium case, we can write this configuration entropy S_c as

$$\frac{S_c}{k_{\mathrm{B}}} = -\sum_{i=1}^{N(\theta)} p^{(i)}(\theta)\ln p^{(i)}(\theta) = \ln\frac{A_{cell}(\theta)}{a_0^2} - \langle\ln\frac{A^{(i)}(\theta)}{a_0^2}\rangle \qquad (1)$$

where $p^{(i)}$ here corresponds to the xne case. Figure 5 shows this configurational entropy for Al, W and Si from our simulations. Note that except for the case of W at low misorientations (below ~20˚), there is a striking similarity in the data amongst the three different materials, except for the overall magnitude, which does appear to be material dependent.

The last expression in Eq. (1) suggests that the entropy can be divided into two parts. The first is associated with A_{cell} and is purely geometric, i.e., it does not depend on material type. We also plot this geometry-dependent term in the entropy $k_B\ln(A_{cell}/a_0^2)$ in Fig. 5 (red curve). The data clearly show that S_c and $k_B\ln(A_{cell}/a_0^2)$ vary with misorientation in a very similar manner (except at small θ in W). This suggests that the second term on the right hand side of the last expression in Eq. (1) is nearly constant (as seen from the blue symbols in Fig. 5) and hence can be written in a θ-independent form as $k_B\ln(\rho a_0^2)$, where ρ is a material parameter we call the "effective density of states". If all $A^{(i)}$ were identical, then $\rho = N/A_{cell}$, i.e., exactly the density of states in $A_{cell}(\theta)$. Here we find that $\rho \approx 7.0a_0^{-2}$, $18.5a_0^{-2}$ and $171a_0^{-2}$

for Al, W and Si, respectively. This again suggests that Si has GBs with the highest structural multiplicity and the degree of structural multiplicity varies from material to material. Based on Eq. (1)

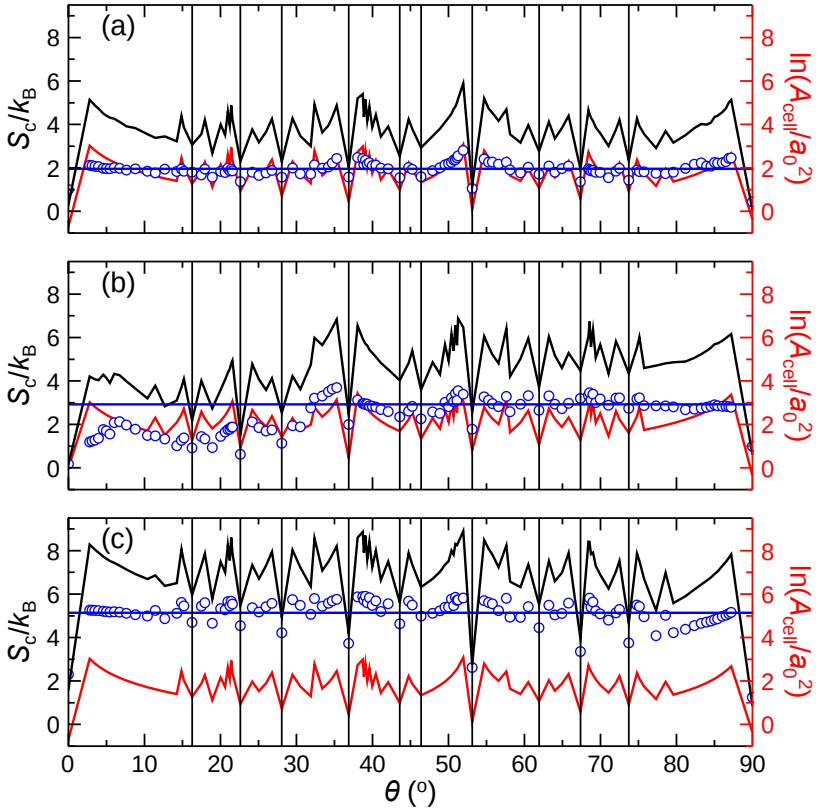

Figure 5. GB configurational entropy of (a) Al, (b) W, and (c) Si as a function of misorientation (black curve) from the data in Fig. 2 and Eq. (1). The dotted red curve and the red axis on the right show the first term in the configurational entropy from Eq. (1). The open blue circles are the result of subtracting the red curve from the black curve, i.e., the second term in Eq. (1).

and employing $A_{cell}/a_0^2 \propto \Sigma^{\beta}$, where β is a constant (β = 1/2 or 1 for symmetrical tilt or twist GBs, respectively), we find that S_C varies linearly with ln Σ.

4. Glass-Like Grain Boundary Behaviour

The extremely high density of metastable grain boundary structures that are close in energy is analogous to the high density of nearly degenerate metastable states that exist in a glass or glass forming liquid. More than 100 years ago, Rosenhain and Ewen [22] postulated that grains in cast iron were "cemented" together by a thin "amorphous" materials ''identical with or at least closely analogous to the condition of a greatly undercooled liquid.'' While there is no doubt today that grain boundary structure is highly ordered [20], this analogy between GBs and glasses (and glass-forming liquids) is persistent [23-28]. Grain boundary properties may indeed exhibit glass or glass-forming liquid like properties; these include GB sliding [27], GB diffusivity [28] and GB mobility [26,28]. Although highly ordered, GB metastable structures constitute a dense spectrum of local states in which GB structure can be trapped. Just as many glass properties are determined by transitions between nearly degenerate states [29], GBs properties kinetic properties may exhibit similar glass-like properties. For example, the Vogel-Fulcher relation provides a much better fit to the temperature-dependence of grain boundary mobility than does the Arrhenius relation (as for relaxation times in glass forming liquids) [26]. We examine this conjecture

via the relationship between the multiplicity of grain boundary states, the configurational entropy, and glass-like relaxation behavior within the framework of Adam-Gibbs theory [30].

Adam-Gibbs theory [30] explains the temperature dependence of the relaxation behavior in glass-forming liquids in terms of the temperature variation of the size of the cooperatively rearranging region in the material. As the temperature is lowered, the system is able to explore smaller and smaller regions of phase space within any fixed time period (e.g., that of a physical measurement). One conclusion from this approach (and many other works since) is that the typical relaxation time τ scales with temperature as $\tau \sim \exp(C/TS_c)$, where C is a constant, T is temperature and S_c is the configurational entropy. For describing grain boundaries, we employ the configurational entropy from Eq. (1). As discussed above, $A_{cell}/a_0^2 \propto \Sigma^{\beta}$ and Σ varies with θ while the effective density of states ρ does not. This implies that the misorientation dependence of the kinetic relaxation time should scale with misorientation θ as

$$\tau(\theta) = \tau_0 e^{C/TS_c(\theta)} = \tau_0 \exp\left[\frac{C'/k_B T}{\ln(A_{cell}(\theta)/a_0^2)+\ln(\rho a_0^2)}\right] = \tau_0 \exp\left[\frac{C'}{k_B T \ln(DA_{cell}(\theta)/a_0^2)}\right] \quad (2a)$$

$$\tau(\theta) = \tau_0 \exp\left[\frac{C''}{k_B T \ln(D\Sigma(\theta))}\right] \quad (2b)$$

where C, C', C'' and D are all constants (independent of θ).

5. Application: defect absorption at grain boundaries

The above analysis demonstrates the connection between the high density of metastable structures in grain boundaries, the configurational entropy and grain boundary kinetics. As a demonstration of the applicability of these results, we consider the variation in structure that occurs at grain boundaries from thermal fluctuations, from adsorption of point defects, and adsorption of point defects at grain boundaries (e.g., during irradiation).

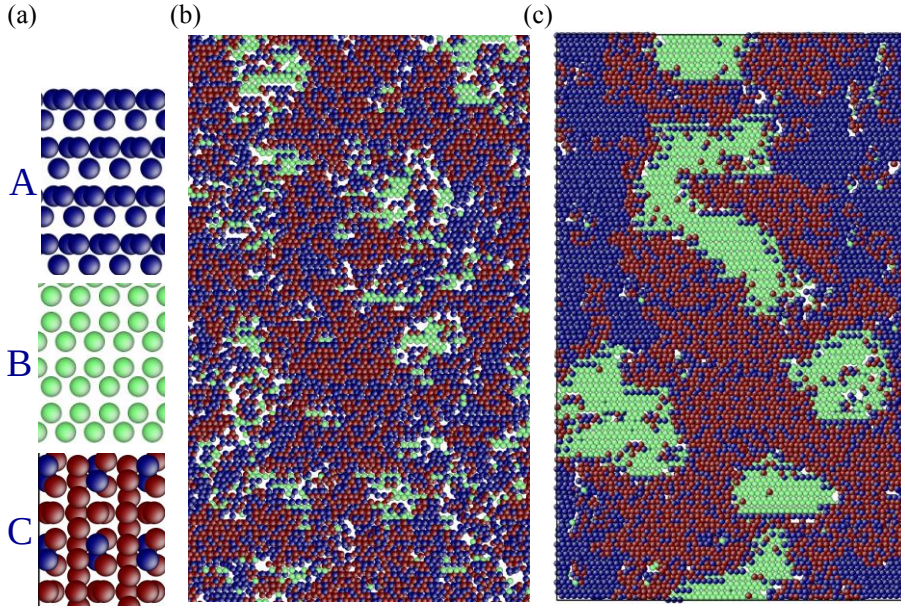

Figure 6. (a) Three different Σ5 (310) [001] symmetric tilt GB structures in W (the labelling A, B, C simply identifies metastable states). The colours label classes of topological type and are arbitrary. (b) An MD simulation cell of a 61,778 Å^2 GB of the same type, equilibrated at 3000 K. (c) Same as (b) but following adsorption of 2400 interstitial atoms into the GB at 1500 K.

In order to distinguish different grain boundary structures, we focus on low Σ boundaries where the number of available states make it possible to distinguish one grain boundary structure from another. We first consider the Σ5 (310) [001] symmetric tilt GB in W, for which there are three distinct metastable structures that we arbitrarily label A, B, and C, as shown in Fig. 6(a). We identify different sites in the bicrystal by finding the Voronoi cell around each atom and labeling each site according to its complete topology [31], and not considering atoms whose Voronoi cell topology corresponds to the BCC crystal lattice. In this way, atoms in different GB structures can be identified [32]. Figure 6(b) shows a 61,778 Å^2 GB of this type, equilibrated at 3000K and quenched to 0K. Examination of the GB shows that the boundary consists of coexisting domains of all three structures. The lowest energy state corresponds to A in Fig. 6(a).

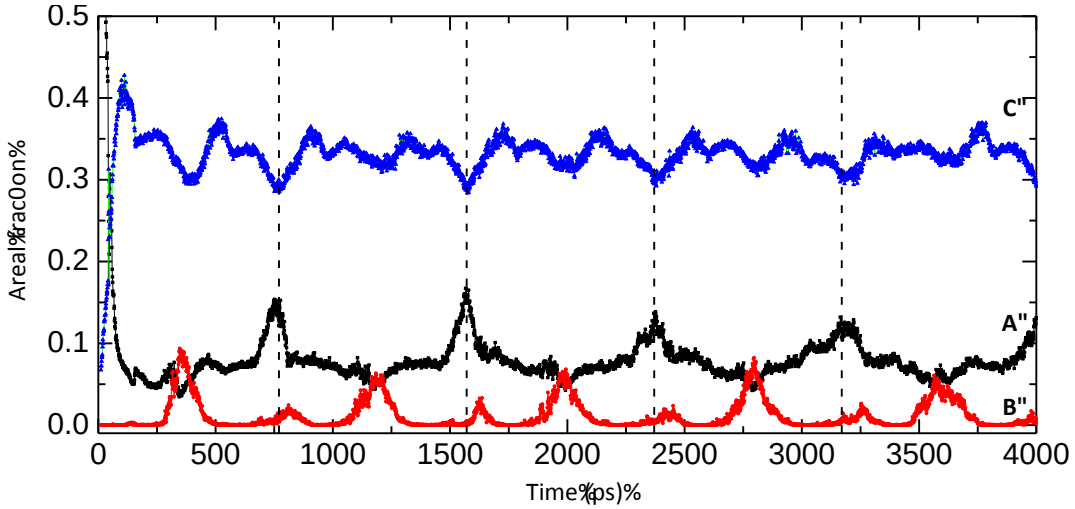

Figure 7. The area fraction of the Σ5 (310) [001] symmetric tilt GB in W of each of the three metastable structure types (A-black, B-red, C-blue curves) shown in Fig. 6(a) as a function of time from a molecular dynamics simulation performed at 1500K where interstitials are introduced into the 61,778 Å^2 boundary at a rate of 10/ps to simulate point defect adsorption at a GB during radiation damage.

Adsorbing 2400 interstitial atoms into the GB in Fig. 6(b) at 1500K transforms this structure into that shown in Fig. 6(c). Compared to the original structure in Fig. 6(a) this grain boundary has larger domains of all three boundary types; likely a result of lowering the temperature. We introduce interstitials into this same grain boundary at a fixed rate during a molecular dynamics simulation at 1500K to simulate point defect annihilation at a grain boundary during irradiation. Figure 7 shows the fraction of the boundary occupied by each of the three structural types shown in Fig. 6(a) as a function of time where interstitials are introduced into the 61,778 Å^2 GB at a rate of 10/ps to simulate point defect adsorption at a GB during radiation damage. We note that the dominant boundary type is C during this dynamic simulation even though type A has the lowest energy. The other interesting feature of these dynamics is that the fraction of the boundary occupied by each type is a nearly periodic function of time. This time period corresponds to that necessary to add the number of interstitials equal to the number of atoms on a single plane parallel to the boundary, since adsorption of this number of interstitials corresponds to the translation of the GB by a single atomic plane (~10^4 W interstitials).

We now turn to the analysis of an experiment in which polycrystalline Cu was irradiated with He ions at elevated temperature [33]. (We note that while the experiments were performed on an FCC metal and the simulations on a BCC metal, the results presented above demonstrate that the main predictions are crystal structure independent in cubic materials.) While dislocation loops and voids formed within grains, regions of near constant width where these defects were nearly absent were found in the vicinity of some grain boundaries but not others. The width of these denuded zones (DZ) varied from GB to GB;

suggesting that some GBs are more efficient point defect sinks than others. We model this process by assuming that the adsorption and incorporation of point defects into GBs leads to the shift of the GB structure between metastable states. To analyze this situation, we return to the Adam-Gibbs theory which suggests that relaxation rates scale with configurational entropy as ~exp(-C/TS_c). From the dependence of the configurational entropy on the metastable state statistics, discussed above, this implies that the adsoprtion rate of point defects should depend on misorientation and through this on Σ. The denuded zone width λ is the compromise between the rate at which point defects diffuse to the grain boundary and the rate at which they can be adsorbed/relaxed into the boundary. During irradiation at a constant rate, a steady-state point defect profile is established such that λ is proportional to the rate of adsorption and hence varies inversely with relaxation time τ. Given the relationship between Σ and τ in Eq. (2b), this implies that $\lambda = \lambda_0 \exp(-F/T \ln\Sigma)$, where F is a constant, or at fixed temperature (as in these experiments), $\lambda = \lambda_0 \exp(-F'/\ln\Sigma)$.

We replot the DZ width λ data from [33] for small Σ versus Σ in Fig. 8. Not surprisingly, the DZ width decreases as Σ decreases, since the fewer metastable states available (typical of low Σ boundaries) the more difficult (longer relaxation times) it is to relax the point defects in the boundaries. We fit the data to the theoretical form from above $\lambda = \lambda_0 \exp(-F'/\ln\Sigma)$ and compare the prediction with the experimental data in Fig. 8. As expected, the model shows that larger-Σ GBs have higher sink efficiency than lower-Σ GBs; this dependence, however, becomes weak for large Σ ($\lambda \rightarrow \lambda_0$ in this limit). The agreement between the GB property prediction and the experimental measurements supports the γ-band model, the underlying GB statistics upon which this prediction rests, and the Adam-Gibbs approach to determining GB relaxation kinetics.

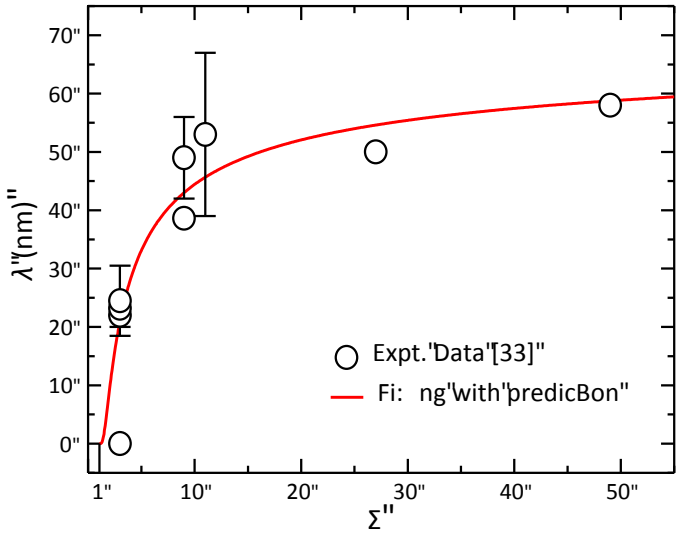

Figure 8. The denuded zone width λ versus the reciprocal coincident site lattice density Σ. The experimental data are from [33] and the red curve is the best fit to those data using, $\lambda = \lambda_0 \exp(-F'/\ln\Sigma)$.

6. Discussion and Conclusions

The results presented above provide compelling evidence from atomistic simulations in three different materials with three different crystal structures that the multiplicity of grain boundary structure is ubiquitous and that the magnitude of this multiplicity is much larger than generally appreciated. While we characterized this multiplicity for a series of [001] symmetric tilt GBs in these materials, we expect that such large multiplicities are the general rule for all crystalline materials and most grain boundaries. Corresponding to this large set of metastable structures for fixed macroscopic degrees of freedom is the broadening of the GB energy versus misorientation curve into a fairly broad and continuous band of

energies versus misorientation. Hence, the common picture of grain boundary thermodynamics is rather oversimplified. The GB energy band versus misorientation can be understood in terms of the structural unit model by admitting multiple possible GB structures at delimiting GBs.

The existence of a large multiplicity of GB states at fixed macroscopic degrees of freedom with a near continuous set of energies suggests that GB configurational entropy S_c should be important for GB properties. We demonstrated that the GB S_c consists of two major contributions, the first is purely geometric and depends on the reciprocal coincident site lattice density Σ and the second is sensitive to bonding and, hence, to material type and crystal structure.

When a large set of metastable states of a particular grain boundary is available, grain boundary dynamics should be sensitive to transitions between nearby metastable states. At high temperature, multiple states should be observable, as expected on the basis of equilibrium thermodynamics. In addition, when grain boundaries are out-of-equilibrium, for example, following a quench or during dynamical processes such as GB sliding, GB migration, and during irradiation, the distribution of GB structures is expected to differ significantly from those observed in equilibrium. This is akin to a liquid where it dynamically shifts between nearly degenerate states. However, GB properties are likely more similar to glass forming liquids where the ability to access other states decreases as the temperature is lowered. In this view, the relaxation dynamics/kinetics of a grain boundary, like a glass-forming liquid, can be described using Adam-Gibbs theory that suggests that relaxation time grows with decreasing temperature or S_c as $\tau \sim \exp(C/TS_c)$.

Using the dependence of GB S_c on the reciprocal coincident site lattice density Σ found in atomistic simulations we can make predictions of how grain boundary relaxation kinetics depends on the five macroscopic GB degrees of freedom. We presented some evidence from a radiation damage scenario that this approach captures the dependence of point defect adsorption kinetics on grain boundary type.

While the results and analysis described herein is a combination of simulation results, statistical mechanics ideas and, admittedly, some speculation, it does provide a new direction in which to think of the relationship between defect structure and defect properties, that is particularly appropriate for 2-dimensional defects, such as GBs, heterophase interfaces and surfaces that are not singular. It also suggests that the renewed attention to structural phase transitions in grain boundaries is interesting, even though most of the extant work only considers extremely simple (near singular) grain boundaries. The more general case is particularly fascinating.

Acknowledgments
The authors gratefully acknowledge Emanuel A Lazar for his assistance in analysing the GB structures in Figs. 6 and 7 and for making his unpublished topological analysis codes available to the authors for this work. JH and DJS gratefully acknowledge the support of the Center for the Computational Design of Functional Layered Materials, an Energy Frontier Research Center funded by the U.S. Department of Energy, Office of Science, Basic Energy Sciences under Award # DE-SC0012575.

References
[1] Bollmann W 1970 *Crystal Defects and Crystalline Interfaces* (Berlin: Springer)
[2] Vitek V 1970 *Scripta Metall*. **4** 725
[3] Bristowe P D and Crocker A G 1975 *Phil. Mag.* **31** 503
[4] Smith D A, Vitek V and Pond R C 1977 *Acta Metall.* **25**, 1363
[5] Pond R C, Smith D A and Vitek V 1979 *Acta Metall.* **27**, 235
[6] Bristowe P D and Crocker A G 1978 *Phil. Mag.* **38A** 487
[7] Olmsted D L, Buta D, Adland A, Foiles S M, Asta M, and Karma A 2011 *Phys. Rev. Lett.* **106**, 046101
[8] Frolov T, Olmsted DL, Asta M and Mishin Y 2013 *Nature Comm.* **4** 1899
[9] Vitek V, Sutton A P, Wang G J and Schwartz D 1983 *Scripta Metal*. **17** 183
[10] von Alfthan S, Haynes P D, Kaski K, and Sutton A P 2006 *Phys. Rev. Lett.* **96** 055505
[11] Vitek V, Minonishi Y, and Wang G J 1985 *J. Phys. (Paris)* **46 C4** 171

[12] Tarnow E, Dallot P, Bristowe P D, Joannopoulos J D, Francis G P, and Payne M C 1990 *Phys. Rev. B* **42** 3644
[13] Krakow W 1991 *Philos. Mag. A* **63** 233
[14] Mills M J, Daw M S, Thom G J and Cosandey F 1992 *Ultramicroscopy* **40** 247
[15] Mishin Y, Farkas D, Mehl M J, and Papaconstantopoulos D A 1999 *Phys. Rev. B* **59** 3393)
[16] Ackland G J and Thetford R 1987 *Philos. Mag. A* **56** 15
[17] Tersoff J 1988 *Phys. Rev. B* **37** 699
[18] Wang G J and Vitek V 1986 *Acta Metall.* **34** 951
[19] Sutton A P and Balluffi 1995 *Interfaces in Crystalline Materials* (Oxford: Oxford University Press)
[20] Sutton A P and Vitek V 1983 *Phil. Trans. Royal Soc. (London) A* **309** 1
[21] Shannon C E 1948 Bell *System Technical Journal* **27** 379
[22] Rosenhain W and Ewen D 1913 *J. Inst. Met.* **10** 119
[23] Ashby M F 1972 *Surf. Sci.* **31** 498
[24] Keblinski P, Phillpot S R, Wolf D, and Gleiter H 1996 *Phys. Rev. Lett.* **77** 2965
[25] Wolf D 2001 *Curr. Opin. Solid State Mater. Sci.* **5** 435
[26] Zhang H, Srolovitz D J, Douglas J F, and Warren J A, *PNAS* **106** 7735
[27] Ke T S 1947 Phys. Rev. **71** 533
[28] Schoenfelder B, Keblinski P, Wolf D and Phillpot S R 1999 *Intergranular and Interphase Boundaries in Materials* (Pfaffikon, Switzerland: TransTech)
[29] Berthier L and Biroli G 2011 *Rev. Mod. Phys.* **83** 587
[30] Adam G and Gibbs J H, 1965 *J. Chem. Phys.* **43** 139
[31] Lazar E A, Mason J K, MacPherson R D, and Srolovitz D J 2012 *Phys. Rev. Lett*. **109** 095505
[32] Lazar E A, Han J, and Srolovitz D J, to be published
[33] Han W Z, Demkowicz M J Fu E G, Wang Y Q, and Misra A 2012 *Acta Mater.* **60** 6341